

Xuan Song

Department of Mechanical
and Industrial Engineering,
The University of Iowa,
3131 Seamans Center,
Iowa City, IA 52242
e-mail: xuan-song@uiowa.edu

Zhuofeng Zhang

Department of Aerospace and
Mechanical Engineering,
University of Southern California,
Los Angeles, CA 90089
e-mail: zhuofenz@usc.edu

Zeyu Chen

Department of Biomedical Engineering,
University of Southern California,
Los Angeles, CA 90089
e-mail: zeyuchen@usc.edu

Yong Chen¹

Epstein Department of Industrial and
Systems Engineering,
University of Southern California,
GER 201, 3715 McClintock Avenue,
Los Angeles, CA 90089
e-mail: yongchen@usc.edu

Porous Structure Fabrication Using a Stereolithography-Based Sugar Foaming Method

Porous structure has wide application in industry due to some of its unique properties such as low density, low thermal conductivity, high surface area, and efficient stress transmission. Both templating and foaming agent methods have been used to fabricate porous structures. However, these methods can only fabricate simple geometries. In recent years, many studies have been done to use additive manufacturing (AM), e.g., stereolithography apparatus (SLA), in the fabrication of porous structure; however, the porosity that can be achieved is relatively small due to the limited accuracy in building microscale features on a large area. This paper presents a projection-based SLA process to fabricate porous polymer structures using sugar particles as the foaming agent. With a solid loading of 50 wt.% of sugar in photocurable resin, the method can achieve a structure with much higher porosity. As shown in our results, the method can increase the porosity of fabricated scaffold structures by two times when compared to the current SLA method. [DOI: 10.1115/1.4034666]

Keywords: stereolithography, sugar foaming, porosity, 3D printing, scaffold, tissue engineering

1 Introduction

There is increasing interest in fabricating porous or foam structures due to many benefits introduced by the interconnected micropores inside the structures, such as low density, low thermal conductivity, high surface area, and efficient stress transmission. By making use of these properties, porous structures have a wide variety of industrial applications such as oil absorption [1,2], heating/electromagnetic/sound shielding [3–5], sensing and energy harvesting [6–10], tissue engineering [11,12], and sandwich structures [13–15]. Some of the applications are shown in Fig. 1. Among them, an important application of porous structures is to serve as a scaffold in tissue engineering. Emerged in the early 1990s, tissue engineering is to conduct tissue/organ repair by transplanting a biofactor (i.e., cells, genes, and/or proteins) within a porous degradable material known as a scaffold [16]. Numerous research studies have indicated that more tissue ingrowth and new bone formation in vivo occurred in areas with higher porosity [17]. Therefore, it is desired to produce a scaffold structure with higher porosity such that the tissue can grow into the scaffold structure more efficiently.

Plenty of research has been done on developing novel processing technologies to fabricate porous structures with desired porosity. The most common approaches of making porous structures include templating methods [18–20] and foaming agent-based methods [1,3,6,21–29]. The templating methods build a porous structure from an existing porous template. The template is then removed by dissolving the entire structure in a certain type of solution. The foaming agent-based methods are the most widely used approach for the preparation of foam structures with high porosity and are usually employed to process polymer and ceramic materials. In the foaming agent-based methods, a specific

type of foaming agents is mixed with matrix materials and a green part is fabricated from the mixture. The green part is then postprocessed to remove the foaming agent in the volume; hence, interconnected pores can be generated in place of the foaming agent. The used foaming agents vary in different research but generally employ heat-decomposable or soluble particles. For example, Choi et al. [1] and McCall et al. [26] use commercially available sugar as foaming agent to make highly porous polymer composite. In their methods, free sugar particles are added directly to uncured polymer composite. After a thin layer is cured from the mixture, the sugar particles are removed by soaking the cured composite layer in hot water, leaving a three-dimensional (3D) isotropic network of air channels in the polymer composite. Both the templating and foaming agent-based methods can achieve high porosity in the fabricated structures. However, these methods can only produce porous structures with simple shapes, such as a thin layer, and have limited capability of fabricating scaffolds with complex 3D shapes for tissue engineering.

Various researches have been conducted to directly fabricate complex hollow structures using additive manufacturing (AM) technologies [30,31]. However, the porosity that can be achieved by AM processes is still limited by their relatively low resolution in fabricating multiscale features. For example, when using the stereolithography apparatus (SLA) process to build a large scaffold structure, the micropores in the final structure are usually smaller than the original design (refer to Fig. 2). Thus, the porosity of the fabricated scaffold structures is limited due to the overcure in both depth and width [32].

In order to increase the porosity of 3D porous scaffold structures fabricated by the SLA process, we present a sugar foaming-based 3D printing method in this research. In the developed process, micro-sugar particles, serving as foaming agent, are mixed with photocurable resin to form a viscous sugar/resin mixture. A desired geometry is then fabricated from the mixture using a projection-based SLA process integrated with tape casting [33]. The fabricated components based on the sugar/resin mixture are

¹Corresponding author.

Contributed by the Manufacturing Engineering Division of ASME for publication in the JOURNAL OF MANUFACTURING SCIENCE AND ENGINEERING. Manuscript received August 17, 2016; final manuscript received August 28, 2016; published online October 6, 2016. Editor: Y. Lawrence Yao.

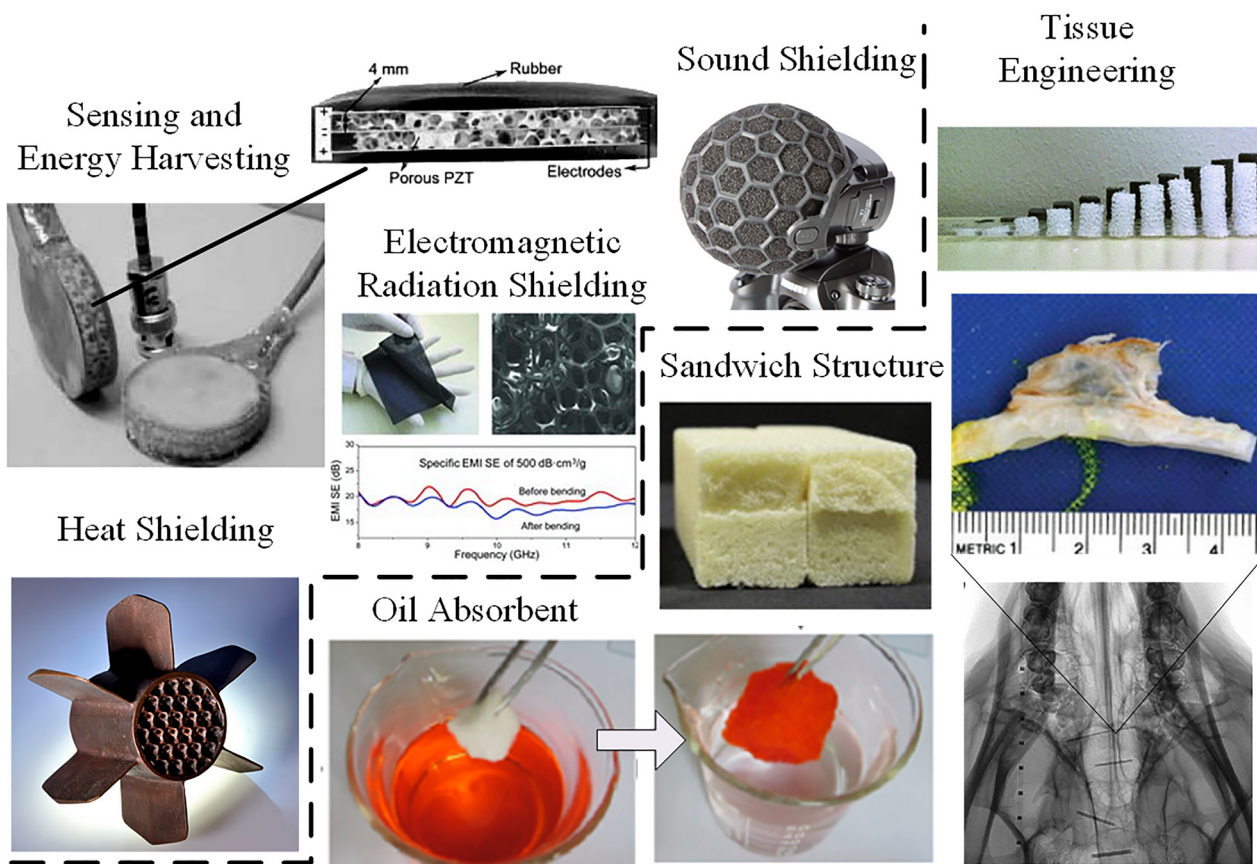


Fig. 1 Applications of various foam structures [1–15]

called *green parts*. To obtain micropores in the green parts, a boiling process is performed afterward. During the boiling process, the green parts are soaked in hot water for a certain amount of time. The sugar particles inside the green parts will gradually dissolve in hot water until porous polymeric structures are obtained. To facilitate the removal of sugar particles in hot water, special patterns are designed for the fabricated green parts. The experimental results show that the porosity of the processed polymer structures can be much higher, which is beneficial to tissue engineering.

The remainder of the paper is organized as follows. The porosity that can be achieved by the regular SLA process is described in Sec. 2. The green part fabrication process and related process parameters such as solid loading, blade coating height, and curing time are discussed in Secs. 3 and 4, respectively. Section 5 discusses the sugar removal process and its limitations including the restriction on sample thickness. Section 6 presents some of the

pattern designs that can support thin features for efficient sugar removal. A test case of a 3D scaffold is presented in Sec. 7. Finally, conclusions with future work are drawn in Sec. 8.

2 Porosity of Scaffold Structures Fabricated by SLA

As shown in Fig. 2, the porosity of an additively manufactured scaffold is usually limited by the relatively low resolution of the

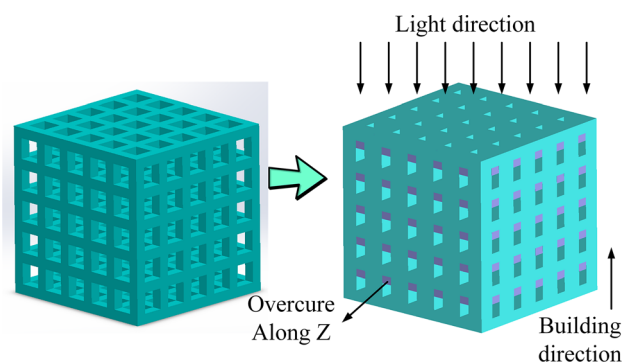


Fig. 2 Limited porosity is achieved by the SLA process due to limited printing resolution and material overcure

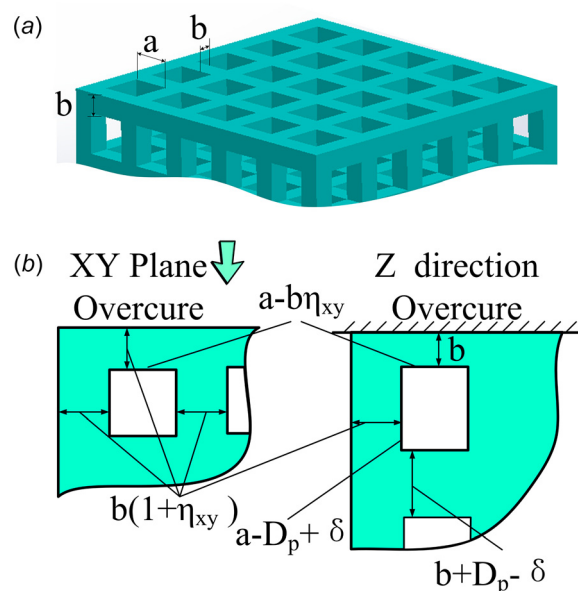


Fig. 3 Porosity calculation: (a) a scaffold design and (b) material overcure in width and depth

AM process. For a scaffold design shown in Fig. 3(a), the ideal porosity ϕ is calculated as

$$\phi = \frac{a^3 n^3 + 3a^2 b n^2 (n+1)}{(n \cdot a + n \cdot b + b)^3} \quad (1)$$

where a is the edge length of pores and b is the width of a strut in the scaffold. The thickness of a single layer of the scaffold is set to b , and the distance between two scaffold layers is a . Assume the number of pores along the x , y , and z directions is the same as n .

When using the SLA process based on a bottom-up projection approach to fabricate scaffold structures, the actual pores will be smaller than the desired size both in the XY plane and along the Z

direction due to the overcure of liquid resin in both width and depth. For simplicity, assume the overcure along the X/Y direction in the XY plane is proportional to the feature's XY lengths with a ratio η_{xy} , and the overcure along the Z direction is equal to $(D_p - \delta)$, which occurs at the overhung features as shown in Fig. 3(b). D_p is the cure depth of the material and δ is the layer thickness. Accordingly, in the actually fabricated structures using the SLA process, the strut width will increase from b to $b(1 + \eta_{xy})$, and the edge length of each pore will decrease from a to $(a - b\eta_{xy})$. The thickness of the first layer of the scaffold keeps constant at b , but all the other layers increase from b to $b + D_p - \delta$ and the distance between two neighboring layers decrease from a to $(a - D_p + \delta)$. Hence, the actual porosity of the fabricated scaffolds can be calculated as

$$\phi = \frac{(a - b\eta_{xy})^2 (bn^2 + bn^3 + an^3) + 2(a - D_p + \delta)(a - b\eta_{xy})b(1 + \eta_{xy})n^2(n+1)}{(n \cdot a + n \cdot b + b + b\eta_{xy})^2 (n \cdot a + n \cdot b + b)} \quad (2)$$

The pore sizes used in scaffolds for tissue engineering are typically designed in the range of 100–600 μm in order to obtain desired outcomes for tissue ingrowth and new bone formation [17]. Hence, the following constraints need to be satisfied for the designed scaffolds:

$$a - b\eta_{xy} \in [100, 600] \mu\text{m}$$

$$a - D_p + \delta \in [100, 600] \mu\text{m}$$

$$\eta_{xy} \in [0, 1]$$

$$\eta_{xy} = f(b)$$

The overcure in the SLA process gives rise to a very low porosity in the directly fabricated scaffolds. For example, in the case of a scaffold with designed pore size $a = 300 \mu\text{m}$, designed strut width $b = 300 \mu\text{m}$, $n = 100$, η_{xy} can be approximately identified by an experiment as 30%, while the actual porosity ϕ can be calculated as 26.5% with a pore size of 200 μm achieved in the finally fabricated structure.

3 Increasing Porosity by Sugar Templating

Traditional porous structure fabrication methods such as the foaming agent-based methods can make simple geometry with increased porosity, while AM technologies including SLA can build complex shapes with a relatively limited porosity. In this research, we present a sugar foaming-based SLA process by combining these two fabrication processes to produce complex scaffold structures with sufficient porosity. In the developed porous structure fabrication process, sugar particles were selected to serve as the foaming agent. The sugar particles used in our study are fine bakery sugar, purchased from King Arthur Flour (Norwich, VT). The size of the sugar particles is around $\sim 150 \mu\text{m}$, which can be dissolved quickly and completely in hot water. The photosensitive resin (SI500 from EnvisionTec, Inc., Dearborn, MI) is used as the matrix material in the experiments. The resin has a viscosity of 180 cP and a density of 1.1 g/cm³ under room temperature [34]. The resin–sugar mixture is prepared in the following steps. First, the sugar is deagglomerated using a mortar and pestle. Afterward, a certain weight ratio of sugar is added in resin and mixed with a stirring rod for 30 min.

The addition of sugar particles into the liquid resin will lead to a dramatically increased viscosity. The current SLA process requires the viscosity of liquid resin to be smaller than 3000 mPa·s [35]. A larger viscosity will make the refill of the material difficult; hence, new layers will not be able to be fabricated successfully. In this research, we use a tape-casting integrated SLA process [33,36] to fabricate green parts from the viscous mixtures. The tape casting is a fabrication process that has been widely used to fabricate ceramic capacitors. We utilize it in our 3D printing process to spread the viscous resin–sugar mixture into a relatively thin layer.

As shown in Fig. 4, when the cycle of fabricating one layer begins, a small amount of resin–sugar mixture is dispensed onto the glass substrate behind the doctor blade. The glass substrate is coated with a Teflon film, which can reduce the attaching force between the photocured layers and the substrate during the layer separation process. Due to its high viscosity, the mixture will not flow out of the substrate. A linear stage is used to move the glass substrate to the left and stop under the building platform. When the viscous slurry is transported beneath the doctor blade, it will be coated into a slurry layer on the transparent glass substrate with a thickness that can be larger than a desired layer thickness. After that, the building platform is moved down along the Z axis to form a gap of one layer thickness above the substrate. Hence, one layer of a 3D structure can be fabricated by projecting a cross section image of the layer onto the bottom of the substrate. Due to the photocurable resin in the resin–sugar mixture, only the paste materials that are within the light-exposed regions are solidified. The cured layer can be uniformly thin since the layer is sandwiched between the previously built layers and the substrate.

To ensure that the newly fabricated layer attaches to the previously built layers, layer separation from the glass substrate is conducted before the cycle of fabricating another layer can be started. In the procedure of layer separation, the glass substrate directly slides toward the right side. As shown in our previous study [37], the sliding mechanism can significantly reduce the force imposed on the cured layer during the separation process to ensure it can be less than the bonding force of the layer with the previously built layers. Consequently, the newly built layer can be successfully detached from the glass substrate. The layer-by-layer building process is repeated until a green part can be fabricated. More details about the green part fabrication process can be found in Refs. [33] and [36]. After the green part is fabricated and removed from the building platform, it is soaked in boiling water for a

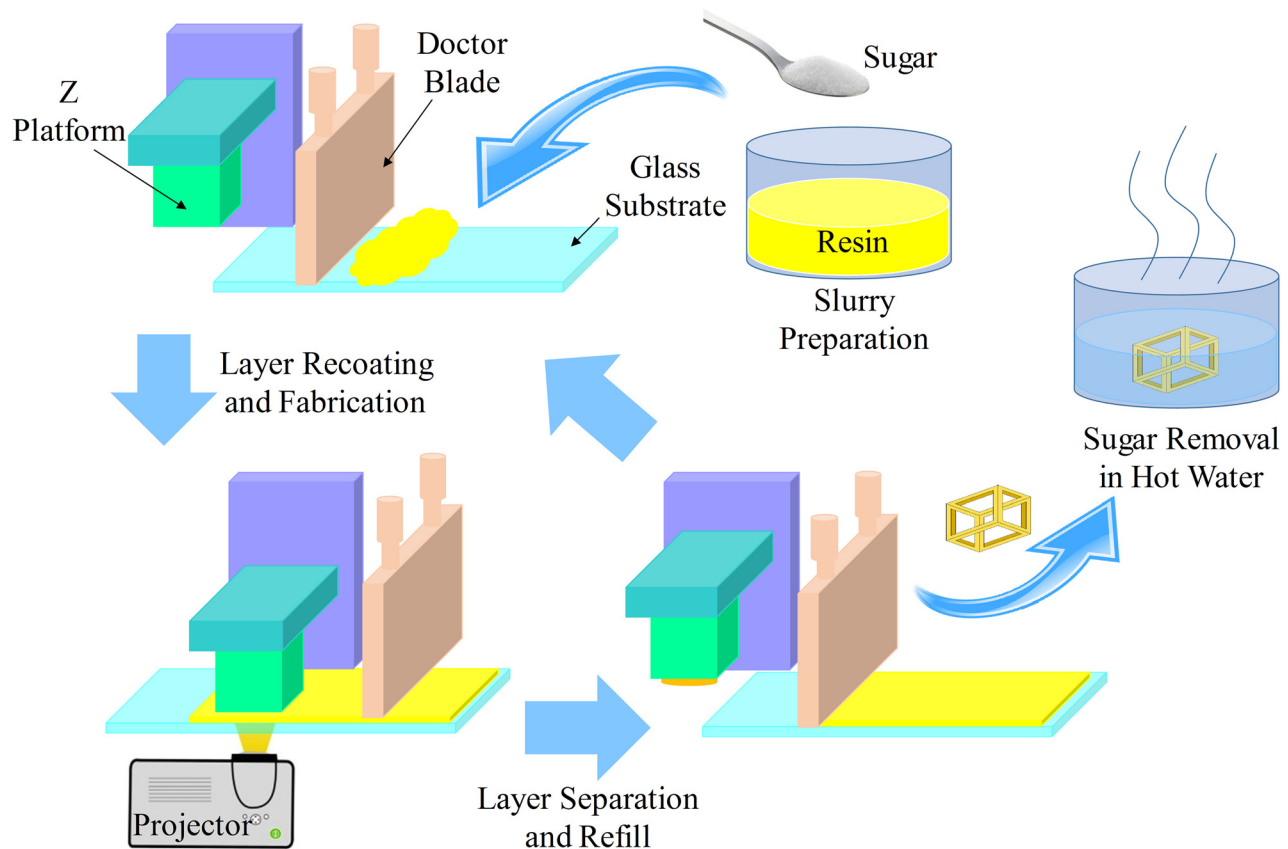


Fig. 4 Schematics of the sugar foaming method based on SLA

certain amount of time. A 3D porous structure can thus be obtained after removing the sugar particles on the part surfaces, as shown in Fig. 5.

4 Main Process Parameters

In this section, we discuss the main process parameters that are associated with the green part fabrication in the sugar foaming-based SLA process. The fabrication of a green part is greatly influenced by the process parameters, such as solid loading of sugar in the mixture, doctor blade height, and curing time used in the SLA process. The effects of the main process parameters as well as the parameter setting methods are discussed as follows.

4.1 Solid Loading Versus Blade Recoating. As mentioned in Sec. 3, a tape-casting process is employed to recoat the resin-sugar mixture into a relatively thin slurry layer. The

recoated slurry layer is required to be uniform and as close to the desired layer thickness as possible. Hence, enough light can pass through the recoated material to solidify the layer, which can tightly bond the previously built layers. Furthermore, after a layer of resin-sugar mixture is recoated on the glass substrate, the building platform moves down to press the recoated slurry layer to form a desired layer thickness. When the thickness of the recoated slurry layer is large, small features on the fabricated green part may be more easily to break when they are pressed down into the recoated layer. To avoid the damage of small features, the layer recoating thickness is preferred to be small. The height of the doctor blade that is raised above the glass substrate is a parameter that determines the thickness of the recoated layer. Literature [33] suggests that the recoated layer thickness is about one-half of the doctor blade height.

In order to fabricate a structure with high porosity, a higher solid loading of sugar is desired in the resin-sugar mixture.

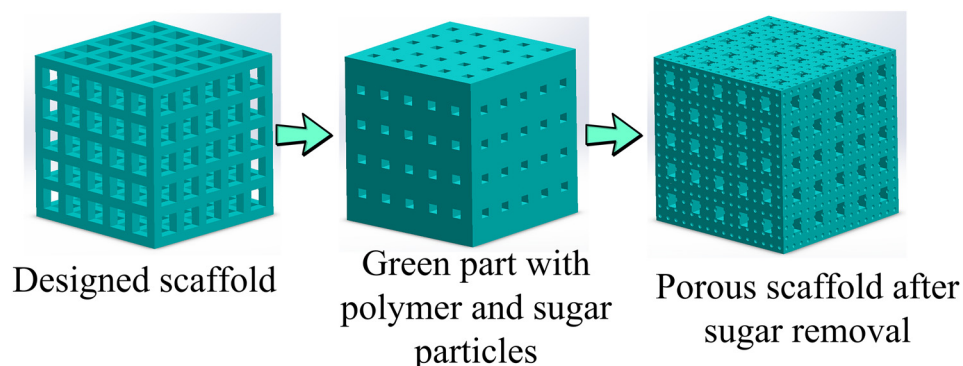

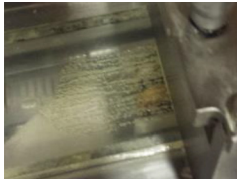













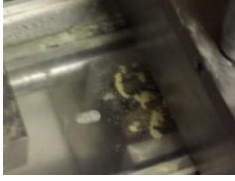


Fig. 5 Increase porosity by the sugar foaming method

Table 1 Slurry coating with different blade heights and solid loadings

Sugar ratio/blade height (mm)	40%	50%	60%	70%
0.2				
0.4				
0.6				
0.8				

However, more sugar gives rise to an increase in the viscosity of the mixture, thus makes the layer recoating more difficult, especially when the height of the doctor blade is small. To identify the optimal solid loading and the related blade height for the resin–sugar mixture, we investigated the slurry recoating under different combinations of sugar ratio and blade height, as shown in Table 1. Four different solid loadings are chosen from 40 wt.% to 70 wt.%. The blade height is set to 0.2 mm, 0.4 mm, 0.6 mm, and 0.8 mm, respectively. The same amount of slurry material was dispensed for each combination of solid loading and blade height. The glass substrate also moves with the same speed beneath the doctor blade. As can be seen in Table 1, a blade height of 0.2 mm is too small to achieve a uniform layer recoating of any solid loadings used in our tests. As the blade height increases, the recoated layer gets thicker but the uniformity also improves. Although a higher solid loading (e.g., 70 wt.%) is desired for an increased

porosity, the recoating process using the designed doctor blade becomes more challenging as well (refer to solid loading 60 wt.% and 70 wt.% in Table 1). Among all the combinations, 50 wt.% sugar ratio and 0.4 mm doctor blade height are the selected setting which leads to the biggest sugar percentage and the smallest recoated layer thickness. In the following experiments in our study, 50 wt.% and 0.4 mm are chosen as the solid loading and the doctor blade height, respectively. The recoating process is fine-tuned to ensure that a thin and uniform layer can be recoated.

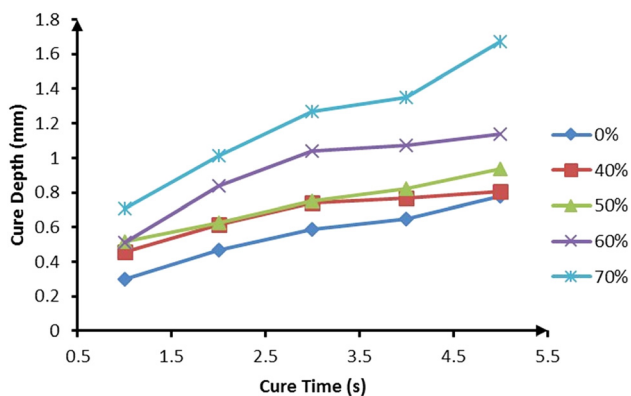


Fig. 6 Cure depth with different cure times for different solid loadings

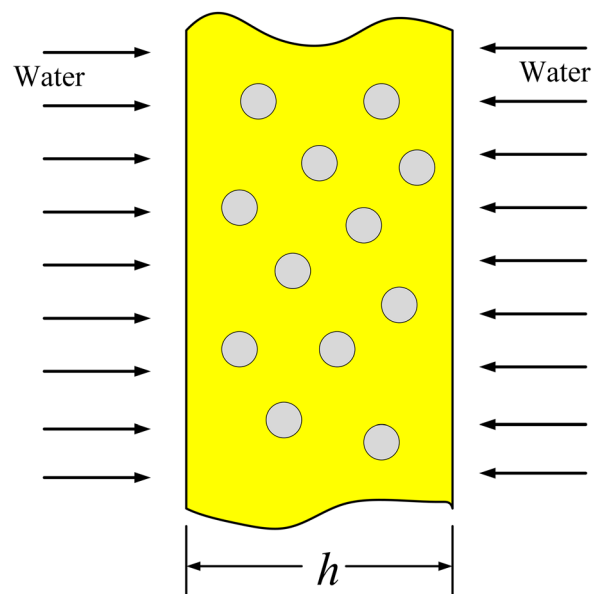


Fig. 7 Description of sugar removal procedure

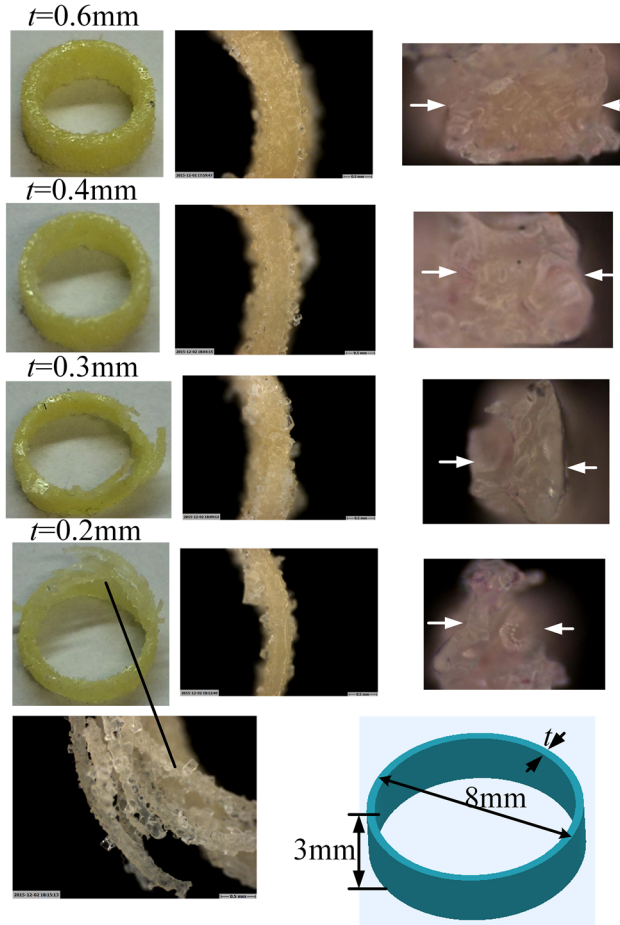


Fig. 8 Cylinder shell structures with different thickness

4.2 Curing Characteristics. To determine the layer thickness to slice a computer-aided design (CAD) model into a set of two-dimensional (2D) layers, curing characteristics of the resin–sugar mixture with different weight ratios are studied. In the experiments, enough slurry with different weight ratios was uniformly spread on the glass substrate. An image of a circle with a diameter of 10 mm was projected onto the bottom of the substrate for a certain amount of time (from 1 s to 5 s) to cure the spread slurry. The thickness of the cured layer was then measured with a microcaliper, which is recorded as the cure depth of the tested slurry material under the given curing time. The measured layer thicknesses (or cure depths) of different slurry materials with respect to different curing time are shown in Fig. 6.

It can be seen in Fig. 6 that the pure resin has the smallest cure depth when compared with the resin–sugar mixture. For the same slurry material, the cure depth increases with the curing time, since more light energy is added for a longer curing time. As the solid loading of sugar in the mixture increases, the cure depth becomes larger. This is because the amount of energy that is absorbed when the light passes through a sugar particle is smaller than the energy that is absorbed when the same light cures the same volume of resin. Hence, the light can go deeper into the slurry with more sugar particles, resulting in a bigger cure depth of the mixture with an increased solid loading. This is significantly different from the slurry with ceramic particles as shown in our previous study [38,39].

5 Sugar Removal

After the structure is fabricated by the presented green part fabrication process, it contains both sugar particles and

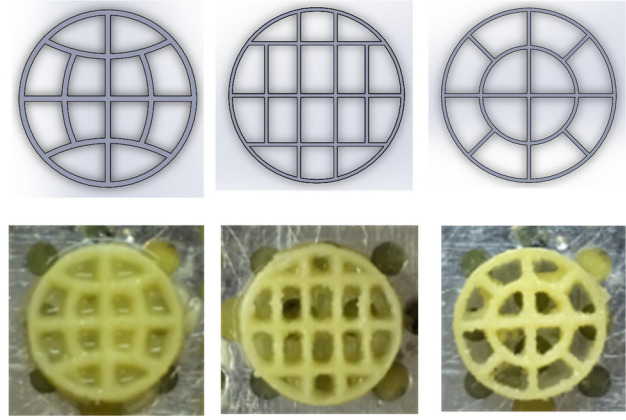


Fig. 9 Different support patterns for thin features

photopolymerized resin. In the following steps, a boiling process is carried out to dissolve the sugar particles in hot water to generate micropores on part surfaces. In order to remove the sugar particles more efficiently, the printed features should be thin enough to expose the sugar particles to hot water; otherwise, some of the sugar particles will be trapped inside the matrix material and will be difficult to be removed during the boiling process. In this section, we discuss the dependence of sugar removal on printed feature sizes.

In our experiment, the green parts were immersed in hot water with a temperature of 80–100 °C. Since the glass transition temperature of the photocurable resin used in our study is 61 °C, the sugar removal procedure can be characterized as Fickian diffusion [40], during which the water diffusion rate is slower than the polymer relaxation rate. Assume a plane sheet of sugar–polymer composite is exposed to the boiling water, as shown in Fig. 7. According to Shen and Springer [41], the percent of water diffusion content M in the plane sheet is modeled as

$$M = G(M_m - M_i) + M_i \quad (3)$$

where M_i is the initial water content of the material, and M_m is the maximum water content after saturation. G is a time-dependent parameter, which can be derived in an approximate form from Fick's second law as [41]

$$G = 1 - \exp \left[-7.3 \left(\frac{D_0 t}{h^2} \right)^{0.75} \right] \quad (4)$$

where D_0 is the water diffusion coefficient in the sugar–polymer composite, t is the boiling time, and h is the sheet thickness.

The diffusion coefficient D_0 can be calculated by referring to the similarities between heat conduction and solution diffusion, which is also used to derive the diffusion coefficient of fiber-reinforced composite in Ref. [41]. For a matrix with randomly distributed spherical fillers [42], the conductivity κ_0 is

$$\kappa_0 = (1 - f)\kappa_1 + f\kappa_2 \quad (5)$$

where κ_1 and κ_2 are the conductivity of the matrix and filler, respectively, and f is the volume fraction of the filler. Analogously, we obtain

$$D_0 = (1 - f)D_1 + fD_2 \quad (6)$$

where D_1 and D_2 are the water diffusion coefficients in polymer and sugar, respectively. We use a cylindrical shell structure (refer to Fig. 8) to study the effect of feature size on sugar removal rate. The outer diameter of the shape is 8 mm. The height of the model

Table 2 Sample weight changes after boiling

Sample thickness (mm)	Weight before boiling w_1 (g)	Weight after boiling w_2 (g)	Porosity after 2 h (%)
0.2	0.057	0.029	58.0
0.3	0.088	0.051	49.7
0.4	0.122	0.064	56.15

is 3 mm. The thickness of the shell changes from 0.2 mm to 0.6 mm. All the fabrication results are shown in columns 1 and 2 in Fig. 8. The cross section of each model after boiling in hot water for 30 minutes is shown in column 3 in Fig. 8. It shows that more sugar particles in 0.2 mm and 0.3 mm shell were removed in water, while not so many voids can be observed in 0.4 mm and 0.6 mm shell. This result suggests that a feature size in a designed scaffold should have a thickness that is no more than 0.3 mm; otherwise, the sugar particles will be trapped inside the polymer.

6 Porous Structure Design for Sugar Removal

As shown in Fig. 8, the shell structures at the thickness of 0.4 mm and 0.6 mm can be successfully fabricated by our process, while some portions of the fabricated shells at the thickness of 0.2 mm and 0.3 mm are broken. It is because shells as thin as 0.2 mm and 0.3 mm are too weak to survive the postprocessing process. However, since the sugar particle size is around 0.15 mm, a smaller feature thickness (e.g., 0.2 mm) is desired in order to remove more sugar particles. To avoid the damage of thinner

features below 0.4 mm, we investigated the design of some patterns to support the weak structures, as shown in Fig. 9. The thickness of the outer shells of the three structures as shown in Fig. 9 is 0.2 mm. The shells have the same diameter as the ones shown in Fig. 8; however, they are rigid due to the inserted pattern designs. The structures with additional patterns can support the thin features and retain the shape of the shell during the fabrication and postprocessing.

To demonstrate the sugar removal of the designed patterns, we used the first pattern design in Fig. 9 to fabricate three structures with a shell thickness of 0.2 mm, 0.3 mm, and 0.4 mm, respectively. All the fabricated parts were cleaned with alcohol in an ultrasonic cleaning machine for 10 min. The cleaned components were then dried in air for 1 h. After that, all the three samples were put in boiling water for 2 h to remove the sugar particles. The weight of each sample was measured before and after the boiling (denoted as w_1 and w_2 , respectively). Assume the weight ratio of the sugar in the mixture is Φ , the density of sugar and resin is ρ_s and ρ_r , respectively. Then, the porosity ϕ of a fabricated structure can be calculated as

$$\phi = \frac{(w_1 - w_2) \cdot \rho_s}{w_1 \cdot \Phi \cdot \rho_s + w_1 \cdot (1 - \Phi) \cdot \rho_r} \quad (7)$$

The measured weights of each sample before and after the boiling process are listed in Table 2. The porosity after boiling for 2 h is calculated using Eq. (7). The density of the sugar used in our experiments is 1.587 g/cm³. As shown in Table 2, the achieved porosity is approximately 58%. The weight change may contain the infiltration of water into polymer and the loss of polymer in the sample during the water boiling process. Both will introduce errors in the calculated porosity: one will decrease the calculated porosity while another will increase it. We believe both factors have limited effect on the weight change. The experimental results suggest an increase of porosity in the final parts. Similar ratios of weight loss in the three samples also suggest that the weight loss of polymer should be small. The micropores that were generated after the removal of sugar particles are shown in Fig. 10(b).

7 Test Results

The sugar foaming-based SLA method can further increase the porosity of a fabricated scaffold compared to the regular SLA process. Assume the actual porosity that can be achieved by the SLA process is ϕ_a . As shown in Sec. 6, a porosity of $\phi_{\text{sugar}} = 50\%$ can be obtained using our sugar foaming-based SLA process. Accordingly, the combined porosity after applying the sugar foaming method to the designed scaffold structure is

$$\phi_a + \phi_{\text{sugar}} - \phi_a \phi_{\text{sugar}} \quad (8)$$

Hence, the incremental ratio δ of the final porosity with respect to the one that is fabricated by the traditional SLA process is

$$\delta = \frac{\phi_{\text{sugar}}}{\phi_a} - \phi_{\text{sugar}} \quad (9)$$

When $\phi_{\text{sugar}} = 50\%$ and $\phi_a = 26.5\%$ as calculated in the above example, the ratio δ can be as high as 138.7%, which is five times higher than ϕ_a .

A more complex scaffold design using the 65 wt.% glass slurry (sodium aluminosilicate glasses, Z-CEL 8054, Potters, Valley Forge, PA) is shown in Fig. 11 to demonstrate the use of the sugar foaming method in fabricating 3D porous scaffold structures. The reason to select the composite is that a relatively large cure depth ($\sim 590 \mu\text{m}$) can be achieved when compared with the sugar particle size. The glass composite was mixed with sugar particles at a weight ratio of 40%. The layer thickness during the fabrication is set as 200 μm . The green part was soaked in hot water (80 °C) for about 40 min. Figures 11(c) and 11(e) show the microscopic

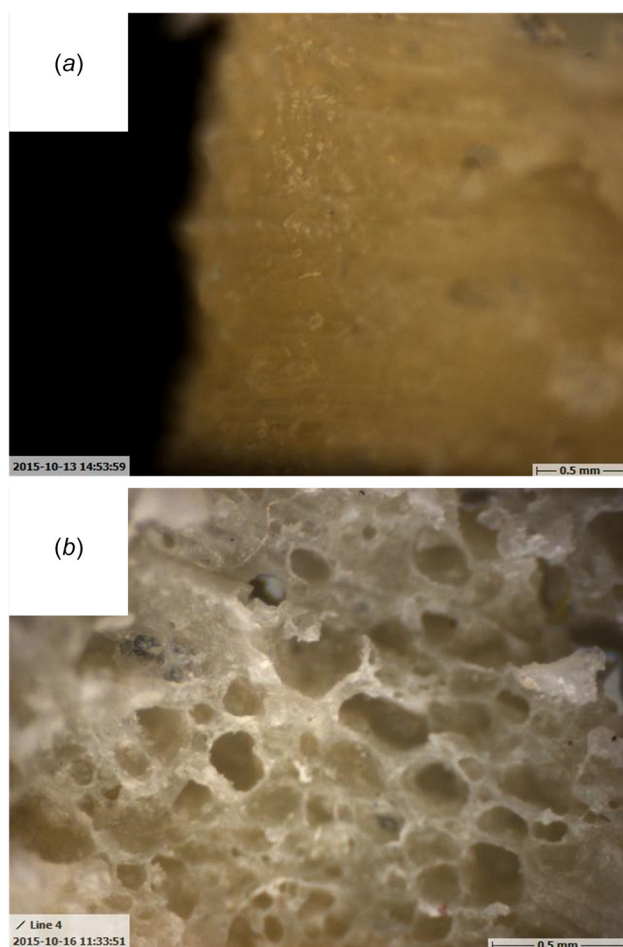


Fig. 10 Microscope image after sugar removal: (a) before boiling and (b) after boiling

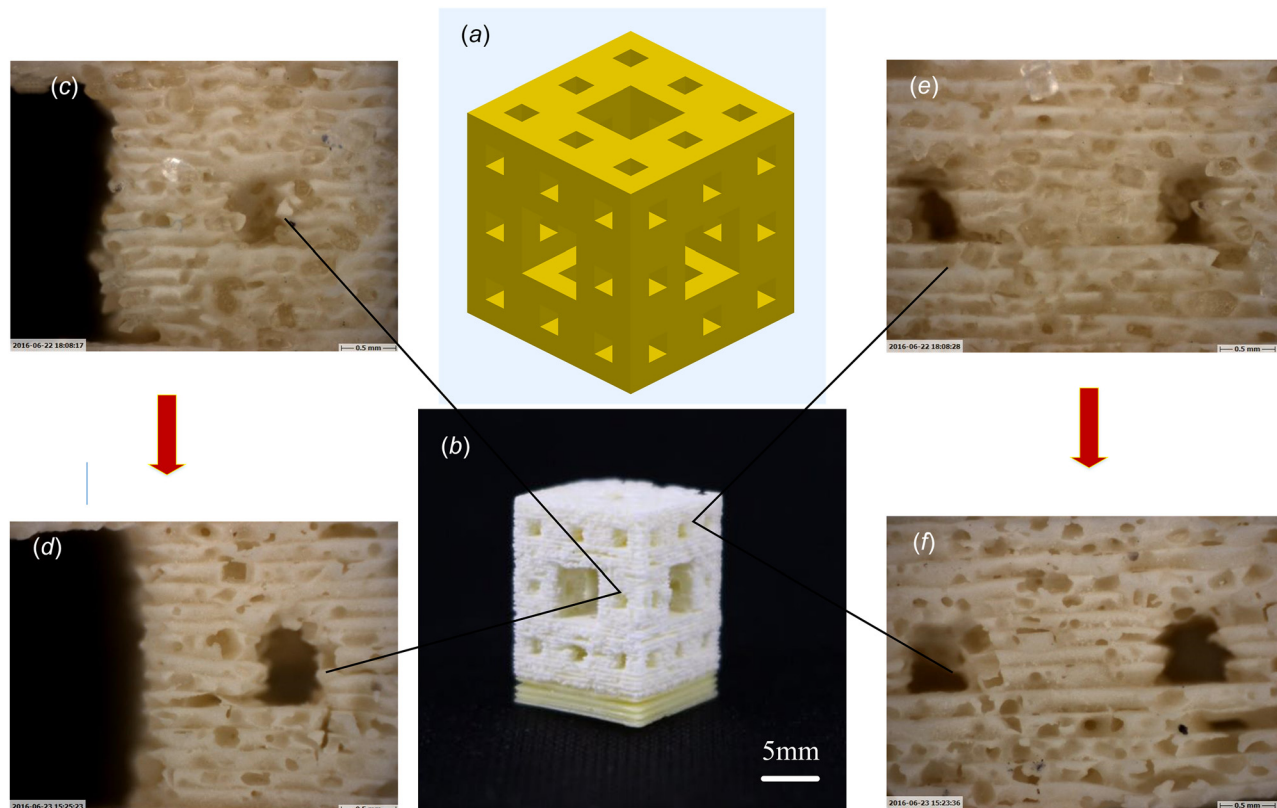


Fig. 11 A glass composite foam structure fabricated by the sugar foaming-based SLA

images of the fabricated green part, in which the semitransparent sugar particles are visible; Figs. 11(d) and 11(f) are the microscopic images of the fabricated polymer structure after the water boiling process, in which the micropores are visible. The weight of the composite scaffold decreases from 1.004 g to 0.783 g after the boiling. The density of the glass composite scaffold is calculated as 1.472 g/cm^3 . From Eq. (7), we can compute the porosity of the final scaffold as 23%. A higher porosity may be obtained by increasing the sugar concentration and the boiling time.

8 Conclusions

This paper presents a sugar foaming-based stereolithography process to fabricate 3D porous structures with complex shapes. The 3D printed material is prepared by mixing the sugar particles with photocurable resin. The mixture is then used in a tape-casting integrated SLA process to fabricate 3D components as green parts. Different process parameters that are important for part fabrication based on the resin–sugar mixture are discussed, including solid loading, blade height, curing time, and layer thickness. In order to remove the sugar particles in green parts more efficiently, a part is designed to have thin features with designed pattern as reinforcement. The sugar particles within the printed green parts are dissolved in boiling water; hence, the micropores can be generated on the surface of the final part. Our experimental results indicate that a weight loss of over 50% can be achieved with the current process parameters leading to the final porosity of scaffolds that is several times higher than that of the traditional SLA process. Thus, the sugar foaming-based SLA process can significantly increase the porosity limit of tissue engineering for scaffolds that can be fabricated by the SLA processes.

In our future research, we will improve the layer recoating process to achieve a higher solid loading in the resin–sugar slurry.

We expect that a higher solid loading of sugar in the mixture will lead to a higher porosity after the boiling process.

Acknowledgment

We thank the support from National Science Foundation (NSF) CMMI-1335476.

References

- [1] Choi, S. J., Kwon, T. H., Im, H., Moon, D. I., Baek, D. J., Seol, M. L., Duarte, J. P., and Choi, Y. K., 2011, "A Polydimethylsiloxane (PDMS) Sponge for the Selective Absorption of Oil From Water," *ACS Appl. Mater. Interfaces*, **3**(12), pp. 4552–4556.
- [2] Zhang, A., Chen, M., Du, C., Guo, H., Bai, H., and Li, L., 2013, "Poly (Dimethylsiloxane) Oil Absorbent With a Three-Dimensionally Interconnected Porous Structure and Swellable Skeleton," *ACS Appl. Mater. Interfaces*, **5**(20), pp. 10201–10206.
- [3] Chen, Z., Xu, C., Ma, C., Ren, W., and Cheng, H. M., 2013, "Lightweight and Flexible Graphene Foam Composites for High-Performance Electromagnetic Interference Shielding," *Adv. Mater.*, **25**(9), pp. 1296–1300.
- [4] Matthieu, B., 2010, "Heat Sink Copper Foam," *Wikimedia Commons*, San Francisco, CA.
- [5] Videomaker, 2015, "Rode Stereo Videomic X Review," *Videomaker, Inc.*, Chico, CA.
- [6] Marselli, S., Pavia, V., Galassi, C., Roncari, E., Craciun, F., and Guidarelli, G., 1999, "Porous Piezoelectric Ceramic Hydrophone," *J. Acoust. Soc. Am.*, **106**(2), pp. 733–738.
- [7] Cha, S., Kim, S. M., Kim, H., Ku, J., Sohn, J. I., Park, Y. J., Song, B. G., Jung, M. H., Lee, E. K., Choi, B. L., and Park, J. J., 2011, "Porous PVDF as Effective Sonic Wave Driven Nanogenerators," *Nano Lett.*, **11**(12), pp. 5142–5147.
- [8] Kara, H., Ramesh, R., Stevens, R., and Bowen, C. R., 2003, "Porous PZT Ceramics for Receiving Transducers," *IEEE Trans. Ultrason. Ferroelectr. Freq. Control*, **50**(3), pp. 289–296.
- [9] Boumchedda, K., Hamadi, M., and Fantozzi, G., 2007, "Properties of a Hydrophone Produced With Porous PZT Ceramic," *J. Eur. Ceram. Soc.*, **27**(13), pp. 4169–4171.
- [10] Lin, C. T., Liao, L. D., Liu, Y. H., Wang, I. J., Lin, B. S., and Chang, J. Y., 2011, "Novel Dry Polymer Foam Electrodes for Long-Term EEG Measurement," *IEEE Trans. Biomed. Eng.*, **58**(5), pp. 1200–1207.

- [11] Hutmacher, D. W., 2000, "Scaffolds in Tissue Engineering Bone and Cartilage," *Biomaterials*, **21**(24), pp. 2529–2543.
- [12] Rodriguez, J. N., Yu, Y. J., Miller, M. W., Wilson, T. S., Hartman, J., Clubb, F. J., Gentry, B., and Maitland, D. J., 2012, "Opacification of Shape Memory Polymer Foam Designed for Treatment of Intracranial Aneurysms," *Ann. Biomed. Eng.*, **40**(4), pp. 883–897.
- [13] Daniel, I. M., and Cho, J. M., 2011, "Characterization of Anisotropic Polymeric Foam Under Static and Dynamic Loading," *Exp. Mech.*, **51**(8), pp. 1395–1403.
- [14] Hung, T. C., Huang, J. S., Wang, Y. W., and Lin, K. Y., 2014, "Inorganic Polymeric Foam as a Sound Absorbing and Insulating Material," *Constr. Build. Mater.*, **50**, pp. 328–334.
- [15] Patrick, J. F., Sottos, N. R., and White, S. R., 2012, "Microvascular Based Self-Healing Polymeric Foam," *Polymer*, **53**(19), pp. 4231–4240.
- [16] Hollister, S. J., 2005, "Porous Scaffold Design for Tissue Engineering," *Nat. Mater.*, **4**(7), pp. 518–524.
- [17] Karageorgiou, V., and Kaplan, D., 2005, "Porosity of 3D Biomaterial Scaffolds and Osteogenesis," *Biomaterials*, **26**(27), pp. 5474–5491.
- [18] Chen, S., He, G., Hu, H., Jin, S., Zhou, Y., He, Y., He, S., Zhao, F., and Hou, H., 2013, "Elastic Carbon Foam Via Direct Carbonization of Polymer Foam for Flexible Electrodes and Organic Chemical Absorption," *Energy Environ. Sci.*, **6**(8), pp. 2435–2439.
- [19] Shastri, V. P., Martin, I., and Langer, R., 2000, "Macroporous Polymer Foams by Hydrocarbon Templating," *Proc. Natl. Acad. Sci. U.S.A.*, **97**(5), pp. 1970–1975.
- [20] Lee, D., Lee, J., Kim, J., Na, H. B., Kim, B., Shin, C. H., Kwak, J. H., Dohnalkova, A., Grate, J. W., Hyeon, T., and Kim, H. S., 2005, "Simple Fabrication of a Highly Sensitive and Fast Glucose Biosensor Using Enzymes Immobilized in Mesocellular Carbon Foam," *Adv. Mater.*, **17**(23), pp. 2828–2833.
- [21] Ramay, H. R., and Zhang, M., 2003, "Preparation of Porous Hydroxyapatite Scaffolds by Combination of the Gel-Casting and Polymer Sponge Methods," *Biomaterials*, **24**(19), pp. 3293–3302.
- [22] Fukasawa, T., Ando, M., Ohji, T., and Kanzaki, S., 2001, "Synthesis of Porous Ceramics With Complex Pore Structure by Freeze-Dry Processing," *J. Am. Ceram. Soc.*, **84**(1), pp. 230–232.
- [23] Liao, C. J., Chen, C. F., Chen, J. H., Chiang, S. F., Lin, Y. J., and Chang, K. Y., 2002, "Fabrication of Porous Biodegradable Polymer Scaffolds Using a Solvent Merging/Particulate Leaching Method," *J. Biomed. Mater. Res.*, **59**(4), pp. 676–681.
- [24] Mikos, A. G., Thorsen, A. J., Czerwonka, L. A., Bao, Y., Langer, R., Winslow, D. N., and Vacanti, J. P., 1994, "Preparation and Characterization of Poly (L-Lactic Acid) Foams," *Polymer*, **35**(5), pp. 1068–1077.
- [25] Hou, Q. P., Grijpma, D. W., and Feijen, J., 2003, "Porous Polymeric Structures for Tissue Engineering Prepared by a Coagulation, Compression Moulding and Salt Leaching Technique," *Biomaterials*, **24**(11), pp. 1937–1947.
- [26] McCall, W. R., Kim, K., Heath, C., La Pierre, G., and Sirbulu, D. J., 2014, "Piezoelectric Nanoparticle-Polymer Composite Foams," *ACS Appl. Mater. Interfaces*, **6**(22), pp. 19504–19509.
- [27] Lin, Q., Luo, B., Qu, L., Fang, C., and Chen, Z., 2013, "Direct Preparation of Carbon Foam by Pyrolysis of Cyanate Ester Resin at Ambient Pressure," *J. Anal. Appl. Pyrolysis*, **104**, pp. 714–717.
- [28] Dey, A., Kayal, N., and Chakrabarti, O., 2011, "Preparation of Porous SiC Ceramics by an Infiltration Technique," *Ceram. Int.*, **37**(1), pp. 223–230.
- [29] Bai, C. Y., Deng, X. Y., Li, J. B., Jing, Y. N., Jiang, W. K., Liu, Z. M., and Li, Y., 2014, "Fabrication and Properties of Cordierite–Mullite Bonded Porous SiC Ceramics," *Ceram. Int.*, **40**(4), pp. 6225–6231.
- [30] Gauvin, R., Chen, Y. C., Lee, J. W., Soman, P., Zorlutuna, P., Nichol, J. W., Bae, H., Chen, S., and Khademhosseini, A., 2012, "Microfabrication of Complex Porous Tissue Engineering Scaffolds Using 3D Projection Stereolithography," *Biomaterials*, **33**(15), pp. 3824–3834.
- [31] Cooke, M. N., Fisher, J. P., Dean, D., Rinnac, C., and Mikos, A. G., 2003, "Use of Stereolithography to Manufacture Critical-Sized 3D Biodegradable Scaffolds for Bone Ingrowth," *J. Biomed. Mater. Res., Part B*, **64**(2), pp. 65–69.
- [32] Song, X., and Chen, Y., 2012, "Joint Design for 3-D Printing Non-Assembly Mechanisms," *ASME Paper No. DETC2012-71528*.
- [33] Song, X., Chen, Y., Lee, T. W., Wu, S., and Cheng, L., 2015, "Ceramic Fabrication Using Mask-Image-Projection-Based Stereolithography Integrated With Tape-Casting," *J. Manuf. Processes*, **20**, pp. 456–464.
- [34] EnvisionTEC, 2008, "SI500 Technical Data," *Envisiontec, Inc.*, Dearborn, MI.
- [35] Griffith, M. L., and Halloran, J. W., 1996, "Freeform Fabrication of Ceramics Via Stereolithography," *J. Am. Ceram. Soc.*, **79**(10), pp. 2601–2608.
- [36] Song, X., Chen, Z., Lei, L., Shung, K., Zhou, Q., and Chen, Y., "Piezoelectric Component Fabrication Using Projection-Based Stereolithography of Barium Titanate Ceramic Suspensions," *Rapid Prototyping J.*, **23**(1) (in press).
- [37] Pan, Y., Zhou, C., and Chen, Y., 2012, "A Fast Mask Projection Stereolithography Process for Fabricating Digital Models in Minutes," *ASME J. Manuf. Sci. Eng.*, **134**(5), p. 051011.
- [38] Chen, Z., Song, X., Lei, L., Chen, X., Fei, C., Chiu, C. T., Qian, X., Ma, T., Yang, Y., Shung, K., and Chen, Y., 2016, "3D Printing of Piezoelectric Element for Energy Focusing and Ultrasonic Sensing," *Nano Energy*, **27**, pp. 78–86.
- [39] Yang, Y., Chen, Z., Song, X., Zhu, B., Hsiai, T., Wu, P. I., Xiong, R., Shi, J., Chen, Y., Zhou, Q., and Shung, K. K., 2016, "Three Dimensional Printing of High Dielectric Capacitor Using Projection Based Stereolithography Method," *Nano Energy*, **22**, pp. 414–421.
- [40] Masaro, L., and Zhu, X. X., 1999, "Physical Models of Diffusion for Polymer Solutions, Gels and Solids," *Prog. Polym. Sci.*, **24**(5), pp. 731–775.
- [41] Shen, C. H., and Springer, G. S., 1976, "Moisture Absorption and Desorption of Composite Materials," *J. Compos. Mater.*, **10**(1), pp. 2–20.
- [42] Klemens, P. G., 1990, "Thermal Conductivity of Composites," *Int. J. Thermophys.*, **11**(5), pp. 971–976.